Analysis of Long-term Trends and Variability of Sea Surface Chlorophyll-a and Temperature in The Northern Papua Sea, Indonesia

Muhammad Ridwan Ramadhan[1]

[1] Oceanography Study Program, Bandung Institute of Technology, Cirebon, West Java, Indonesia

ridwanramadhan8585@gmail.com

(https://orcid.org/0009-0002-1347-4224)

Abstract

Chlorophyll-a serves as an important proxy for marine ecological productivity, and its dynamics playing pivotal role in the marine productivity, especially within the coral biodiversity hotspot such as Coral Triangle's Northern Papua Sea (NPS). Consequently, elucidating the dynamics in such region is essential. This work aims to investigate the long-term trends and variability of the sea surface chlorophyll-a (SSC). Concurrently, sea surface temperature (SST) was also analyzed to quantify its influence on, and relationship with, observed SSC pattern. Employing over two decades (1998-2023) of satellite observations sourced by Copernicus Marine Service (CMS), advanced statistical techniques were used, including Mann-Kendall (MK) test, continuous wavelet transforms (CWT), cross wavelet transforms (XWT) to investigate the dominant modes of both parameters. The results of this study show a negative correlation between SST and SSC (r=-0.22), in addition, the highest lag correlation results were obtained for 2 months with a correlation value of 0.31. SST variability shows significant periodicity in the semi-annual period (~4-8 months). On the other hand, SSC displays a very different pattern, where significant periodicity variability is produced on an intraseasonal to semi-annual scale (~0-16 months) and a strong interannual signal (~12-16 months). The findings in this study indicate the sensitivity of the Northern Papua Sea to thermal variability caused by the ENSO forcing and indicate the need for further research on chlorophyll-a dynamics equipped with in-situ data, as well as vertical chlorophyll-a analysis to better understand its dynamics.

Keywords: Sea surface chlorophyll-a · Sea surface temperature · Coral Triangle · Northern Papua Sea · Long-term Trends

1. Introduction

Phytoplankton is the most fundamental organism of the marine ecosystems. With chlorophyll-a as a key their photosynthetic pigment, they have overarching role in primary productivity, carbon sequestration, and the conversion inorganic nutrients into organic matter. This foundational process is not only crucial for the intricate marine food webs but also positions important role of phytoplankton in the global biogeochemical cycling (Falkowski, 1994; Litchman et al., 2015). Notably, these organisms are responsible for approximately half of the Earth's primary production (Naselli-Flores & Padisák, 2022), sequestering atmospheric carbon dioxide on a scale comparable to terrestrial biomes, and thus playing a significant role in climate regulation. Given these crucial roles, the ability to accurately monitor and comprehend the intricate dynamics of phytoplankton is paramount for investigating overall ocean health and productivity, making prediction in response to anthropogenic activity and ensuring optimized and sustainable marine resource management.

Advances in satellite monitoring technology has sparked a renaissance in ocean monitoring methodology, particularly in the monitoring of critical variables situated on the sea surface. Crucial ocean parameters such as SST and SSC, which are crucial in understanding ocean and climate dynamics, can now be monitored across wide scale of ocean basins over multi-decadal timescales (Garnesson et al., 2019; Groom et al., 2019). The resulting dataset isn't only allowing us to characterize the long-term spatiotemporal variability but also enable us to extract long-term trends and variability. For instance, Harvey et al. (2015) utilized satellite data to measure SSC and nonalgal suspended particulate matter to predict the turbidity of coastal waters. Furthermore, Chust et al. (2021) used SST data to measure the climate regime shift in the Bay of Biscay, which the findings suggest the SST warming trend have impacted the marine productivity and biodiversity.

Sea surface temperature (SST) serves a physical parameter that has governing influence on phytoplankton through multifaceted pathways. The main mechanism involves the modulation of mixed layer depth—increasing SST is typically associated with water column stratification (Deser et al., 2003), thus affecting the overall profile and thereby inhibiting the vertical mixing and isolating the flux of essentials nutrient from deeper layers (Gittings et al., 2018). In many ocean regions, particularly in oligotrophic waters, nutrients are scarce and thus became the primary limiting factor in primary productivity (Vridik & Tranvik, 2006; Bonnet et al., 2007), this SST-driven stratification often leads to a discernible reduction in phytoplankton biomass, as it can be reflected in lower SSC. These dynamics frequently manifest in inverse relationship between SST and SSC, especially in tropical and nutrient-poor waters (Chernihovsky et al., 2020). Beyond these effects of modulation in the abundance of SSC, SST can directly affect phytoplankton physiology by governing metabolic rates—including photosynthesis, respiration, and growth—through its underlying biochemical mechanism (De Poll et al., 2013). While it is generally known that phytoplankton growth accelerates with increasing temperature, recent studies higlights strict and variable thermal tolerance of phytoplankton (Anderson et al., 2021; Marañón et al., 2022).

Despite the Northern Papua Sea (NPS) clear ocean dynamics and undisputed ecological significance, a clear understanding of the coupled long-term dynamics of SSC and SST in the region remains insufficiently researched. Even though broader regional research of Indonesian waters offers valuable insights (Napitupulu, 2024; Sachoemar & Yanagi, 2001; Khalil et al., 2009), a comprehensive study employing advanced statistical techniques to elucidate the dominant modes of SSC and SST variability and their response to interannual climate modulator for this region has, to date, been elusive.

Built upon the existing knowledge gap and the ecological significance of the Northern Papua Sea, the scope of this study is threefold. Firstly, is to quantitatively characterize the long-term (1998-2023) trends in both SSC and SST. Secondly, to elucidate the dominant modes of seasonal and interannual variability of both parameters by employing decomposition techniques, and thirdly, to investigate and describe the nature of the coupling relationship between SSC and SST dynamics. To attain these objectives, we employed multi-decadal satellite remote sensing data and various statistical methods as clearly outlined in the next section.

2. Materials and Methods

2.1. Study Area

The Northern Papua Sea (NPS) is located in the western equatorial Pacific. It serves as a strategic sector of the Indonesian blue economy, exclusively assigned to be Indonesian fishery management areas 717. Its geographical position places it at the confluence of major oceanographic and atmospheric systems, notably as a key entrance for the Indonesian Throughflow (ITF) and within the pervasive influence of the Western Pacific Warm Pool (WPWP). The region's hydrographic is shaped by seasonally dynamic New Guinea Coastal Current (NGCC) and Undercurrent (NGUC). Which are essential in water mass transport and the modulation of key physical and biogeochemical fields. The intraseasonal ocean dynamics of NPS is widely known to be modulated by Westerly Wind Bursts (WWBs), which propagates eastward from the Indian Ocean to the western equatorial Pacific. This intraseasonal phenomenon causes the traverse of relatively warm water mass along the NPS during the onset of El Nino (Chen et al., 2015; Fedorov et al., 2015; Hu & Fedorov, 2019), causing intensified coastal upwelling (Waas et al., 2014), and enhanced SST gradient (Hasegawa et al., 2009)

The key environmental settings within NPS are further shaped by the compounding effects or larger climatic phenomenon and more localized dynamics. The El Niño-Southern Oscillation (ENSO) exerts a profound and well-documented influence, profoundly impacting the regional profile of SST, wind patterns, upwelling intensity, sea level and current strengths, with consequent impacts on oceanic productivity. The region's bathymetry is featuring narrow straits and deep basins, which also plays crucial role in shaping the local ocean circulation and water mass modification. Furthermore, its vicinity to large land of New Guinea introduces considerable riverine input, which can deliver freshwater, nutrients, and sediments near coastal zones.

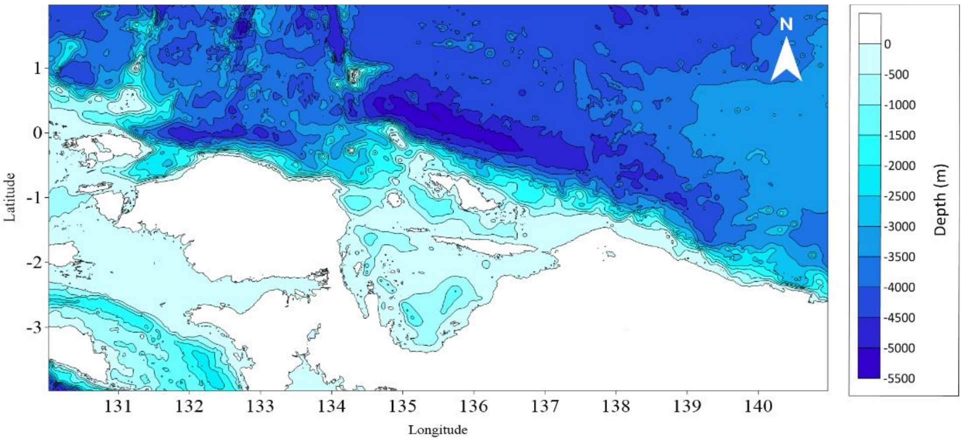

Fig. 1 Study area map

2.2. Data

SSC data were obtained from the Copernicus Marine Service (CMS) global ocean color (Copernicus-GlobColour) Level 4 multi-year product with product ID of OCEANCOLOUR_GLO_BGC_L4_MY_009_104 (doi: https://doi.org/10.48670/moi-00281). This data provides interpolated (gap-free) chlorophyll-a concentrations. For the trend and variability analyses, monthly mean fields at a 4 km native spatial resolution were employed for the period between January 1998 to December 2023. This dataset is a multi-sensor merged product, integrating observations from various ocean color instruments including SeaWiFS, MERIS, MODIS-Aqua, VIIRS-NPP, and OLCI-S3A/B, using sensor-specific algorithms before merging. Global validation against in-situ measurements reports a high coefficient of determination ($r^2 \approx 0.75$) and an RMSD of approximately 0.34 mg/m³ for the daily product.

SST data were also sourced from the CMS global daily gap-free (Level 4) multi-year reprocessed analysis product, specifically IFREMER/ODYSSEA SST_GLO_PHY_L4_MY_010_044 (doi: https://doi.org/10.48670/mds-00345). This dataset provides daily mean SST fields at a horizontal resolution of 0.05°. For this study, data spanning the 26-year period from January 1998 to December 2023 were utilized. This product is derived from a consistent reprocessing of multi-sensor L3 inputs from the European Space Agency Sea Surface Temperature Climate Change Initiative (ESA SST CCI; 1982-2016) and the Copernicus Climate Change Service (C3S; 2017-onwards), ensuring a long-term record. Global validation indicates a bias near zero and an RMSD typically around 0.4-0.5 K.

Oceanic Nino Index were retrieved from NOAA's National Weather Service Climate Prediction Center (https://origin.cpc.ncep.noaa.gov/products/analysis_monitoring/ensostuff/ONI_v5.php) for the period of 1998-2023 which uses 3 month running mean of ERSST.v5 SST anomalies in the Niño 3.4 region (5°N-5°S, 120°-170°W).

Table 1 Data used in the study

Data	Resolution	Source
Sea Surface Temperature (SST)	Daily; 0.05°	CMS
Sea Surface Chlorophyll-a (SSC)	Monthly; 4 km	CMS
Oceanic Nino Index (ONI)	Monthly (3-month running mean)	NOAA

2.3. Methods

2.3.1. Data Preprocessing

To reveal the variability of SSC, a series of data preprocessing steps were systematically applied. the datasets were temporally and spatially harmonized. The daily SST data were temporally aggregated into monthly mean fields to align with the monthly resolution of the SSC and ONI records. To facilitate the analysis of region-wide dynamics, single representative time series were generated by spatially averaging both the monthly mean SST and SSC data over the predefined NPS study area domain (Fig. 1). Finally, to isolate non-seasonal fluctuations and focus on interannual variability, monthly climatologies were computed for both parameters over the full 1998-2023 study period. These long-term monthly means were then subtracted from their respective time series to produce the final monthly anomaly data used in this study. This standard procedure effectively removes the mean seasonal cycle, thereby enabling a clearer characterization of the underlying long-term trends and interannual signals driven by climate phenomena like ENSO.

2.3.2. Characterization of Long-Term Trends

To quantify directional long-term changes, linear trends were computed for the regionally averaged monthly anomaly time series of both SST and SSC. The magnitude of these trends was determined using Sen's slope estimator, and their statistical significance was rigorously assessed using the non-parametric Mann-Kendall (MK) test (Kendall, 1975; Mann, 1945) A significance level of $p < 0.05$ was adopted. For spatially resolved trend analysis, these tests were intended to be applied on a pixel-by-pixel basis to the anomaly data fields. This test was implemented using pyMannKendall library (Shourov & Mahmud, 2019).

The analytical workflow proceeded as follows: for each individual pixel in the study domain, the 26-year monthly anomaly time series was extracted. For each valid pixel-to-pixel time series, the MK test was performed with a significance level set at $\alpha = 0.05$. The classification of the trend at each pixel was then determined using a two-step logic derived from the test's output. First, the significance was established based on the test's boolean result (h), which is true if the calculated p-value is less than 0.05. Second, for pixels identified as having a significant trend, the direction (increasing or decreasing) was assigned based on the sign of the Z-statistic from the test's output. A positive Z-statistic indicated an increasing trend, while a negative Z-statistic indicated a decreasing trend. Pixels where the trend was not statistically significant were classified accordingly. This procedure yielded a spatial map that categorizes the study area into regions of significant increase, significant decrease, or no significant long-term trend.

The mathematical foundations for the test are the S-statistic and the Sen's slope estimator (β). The Mann-Kendall test statistic (S) is calculated as:

$$S = \sum_{k=1}^{n-1} \sum_{j=k+1}^{n} \operatorname{sgn}(x_j - x_k) \qquad (1)$$

where n is the number of data points and $sgn(x)$ is the sign function that determines the relationship between each pair of variables. The magnitude of the trend is then given by Sen's slope estimator (β), which provides a robust estimate of the linear rate of change:

$$\beta = \text{median}\left(\frac{x_j - x_k}{j-k}\right) \qquad (2)$$

Where β is Sen's Slope Estimator which is the median slope of all pairs of data points. This method provides a robust estimate of the true trend slope and is less sensitive to outliers than the regular linear regression method (Pilon & Yue 2004; Henebry & De Beurs 2005).

2.3.3. Unravelling SSC and SST Variability

To calculate the linear relationship between monthly anomalies of SST and ONI with SSC, Pearson correlation analysis is implemented for all three time series data. This method measures the strength and direction of the relationship between two continuous variables. In addition, to identify the presence of a delayed relationship (late response) between the ENSO phenomenon and the SSC response, a lag correlation analysis is also performed, especially between the ONI and SSC time series. The process of applying this lag correlation involves shifting the other variables temporally and calculating the correlation coefficient at each time lag (monthly) to find the maximum correlation. The equation for Pearson correlation can be expressed as:

$$r = \frac{\sum_{i=1}^{n}(x_i-\bar{x})(y_i-\bar{y})}{\sqrt{\sum_{i=1}^{n}(x_i-\bar{x})^2 \sum_{i=1}^{n}(y_i-\bar{y})^2}} \tag{3}$$

Where n is the number of data points, x_i and y_i are the individual values of the two time series, and $\bar{x}$ and $\bar{y}$ are the average values of each time series.

In addition, to explain the regional dynamics and the magnitude of relative SSC fluctuations, the spatial distribution of the Coefficient of Variation (CV) is calculated. CV is calculated as the ratio between the standard deviation (σ) and the mean value (μ), which is often presented as a percentage, with the following formula:

$$CV(\%) = \left(\frac{\sigma}{\mu}\right) \times 100\% \tag{4}$$

2.3.4. Time-Frequency Decomposition of Variability

Continuous Wavelet Transform (CWT) analysis was applied to the regionally averaged monthly anomaly time series of SST and SSC, as well as to the leading PC time series from the EOF analysis. This technique was employed to investigate the temporal evolution of variance across a spectrum of frequencies, identifying dominant periodicities (e.g., seasonal, interannual, decadal) and their modulation over the 1998-2023 period. The Morlet wavelet was selected as the mother wavelet, and the cone of influence (COI) was considered to ensure the robustness of interpretations

$$W_f(a,b) = \int_{-\infty}^{\infty} f(t)\frac{1}{\sqrt{|a|}}\psi^*\left(\frac{t-b}{a}\right)dt \tag{5}$$

In this equation, $W_f(a,b)$ analyzes the time series x(t), a is a scale that determines the higher frequency for lower frequency/longer period; b is the translation or time position; and ψ is the complex conjugate of the parent wavelet used (Morlet wavelet). In addition, the equations used in the implementation of XWT are:

$$W^{XY}(a,b) = W^X(a,b)W^{Y*}(a,b) \tag{6}$$

With $W^{XY}(a,b)$ tests the relationship between two time series by combining their respective CWTs; $W^X(a,b)$ is the CWT of the first series; $W^{Y*}(a,b)$ is the complex conjugate of the second series CWT, both at the same scale a and translation b.

3. Monthly Climatological SSC Level

On synoptic scale, the distribution of SSC (Fig. 2) generally shows relative consistent and uniform distribution of SSC, with relatively high SSC concentration lies near the coast of the Northern Papua, particulary in the southwest and the coast near 138°E which exhibit undulating pattern on monthly basis. In contrast, offshore waters generally exhibit lower SSC values, typically below 0.4 mg/m³, characteristic of more oligotrophic conditions prevalent in the Western Pacific Warm Pool. Based on the monthly temporal evolution, June became the month with highest SSC (0.414 mg/m³); while November became the lowest (0.358 mg/m³). The seasonal fluctuations of SSC in the Northern Papua Sea displays a pronounced cycle, as illustrated by the monthly climatology. During the Austral winter (June-August), elevated SSC concentrations are widespread along the coast and extend further offshore, particularly in southwestern part of the region, which is also proven by elevated SSC concentration level (0.397 mg/m³). During the Austral summer (December-February), SSC concentration near the coast highlights relatively mild decrease compared to austral winter, with spatial mean of 0.359 mg/m³. On the other hand, the first and second transitional season exhibit moderate SSC concentration, with spatial mean of 0.382 and 0.354 mg/m³.

The persistence of relatively higher SSC near the coastal region within the range of 131-134°E and 136-138°E throughout most of the year, albeit with seasonal intensity changes, indicates these areas as potentially consistent zones of enhanced productivity. However, the box plot, as shown on Fig.2, suggests that the SSC concentration across the region experienced temporally variable SSC level strengthening/weakening, suggesting that there might be factors confluencing the SSC dynamics on another periodicity. The potential factor influencing the dynamics of the productivity suggests that multifaceted factors may partake in this phenomenon. Napitupulu (2024) analyzed high activity in seasonal winds during the boreal winter season which in turns intensify coastal upwelling across the region. The spatiotemporal signature of higher SSC being aligned with specific coastal segments might correspond to the primary outflow regions of these rivers or areas consistently influenced by their plumes. For instance, major rivers such as the Mamberano river which is located in the middle of the study area landmass deliver freshwater, terrigenous sediments, and dissolved and particulate nutrients to the coastal environment (Dwirastina & Atminarso 2021).

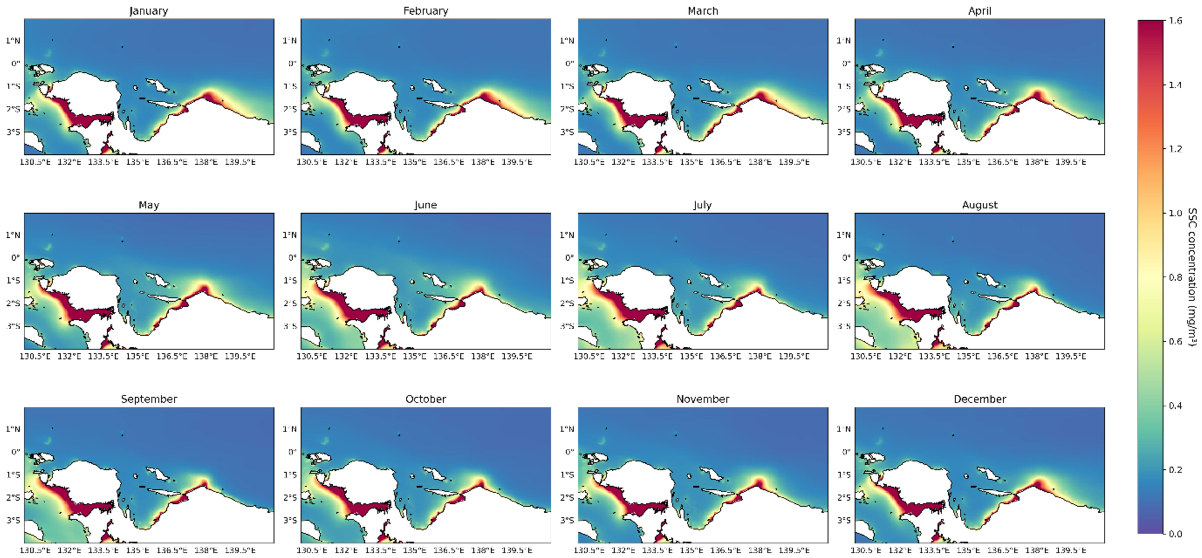

Fig. 2 Spatial distribution of monthly climatological SSC concentration

Advancing beyond the mean seasonal cycle, the monthly year-to-year SSC level provide deep insights into the temporal heterogeneity and interannual predictability of the regional phytoplankton dynamics (Fig. 3). The plot suggest that the period of highest average productivity (May-July) is concurrently the period of lowest year-to-year predictability. This is proven by the large Interquartile Range (IQR) observed during these months, particularly in June, where the IQR reaches its annual maximum of approximately 0.039 mg/m³. This considerable spread, along with the extensive whiskers indicates that while the occurrence of a summer bloom is a reliable feature, its intensity is highly inconsistent from one year to the next, suggesting a strong sensitivity to the varying strength of interannual drivers during this season.

In contrast, the seasonal trough in April and November exhibit the highest degree of consistency. The IQR during these months is at its annual minimum, with respective IQR of 0.029 mg/m³ and 0.025 mg/m³, less than 60% of the June value, indicating that the ecosystem reliably returns to a stable, low-biomass state with minimal year-to-year fluctuation. This suggests the baseline oligotrophic condition is a robust and predictable feature of the regional ecosystem during the transitional season. However, despite the low IQR exhibited by both months, the presence of outlier, as presented by anomalous high and low concentration event observed in April, highlights the system's susceptibility to sporadic, anomalous forcing that can occasionally disrupt the expected seasonal fluctuations.

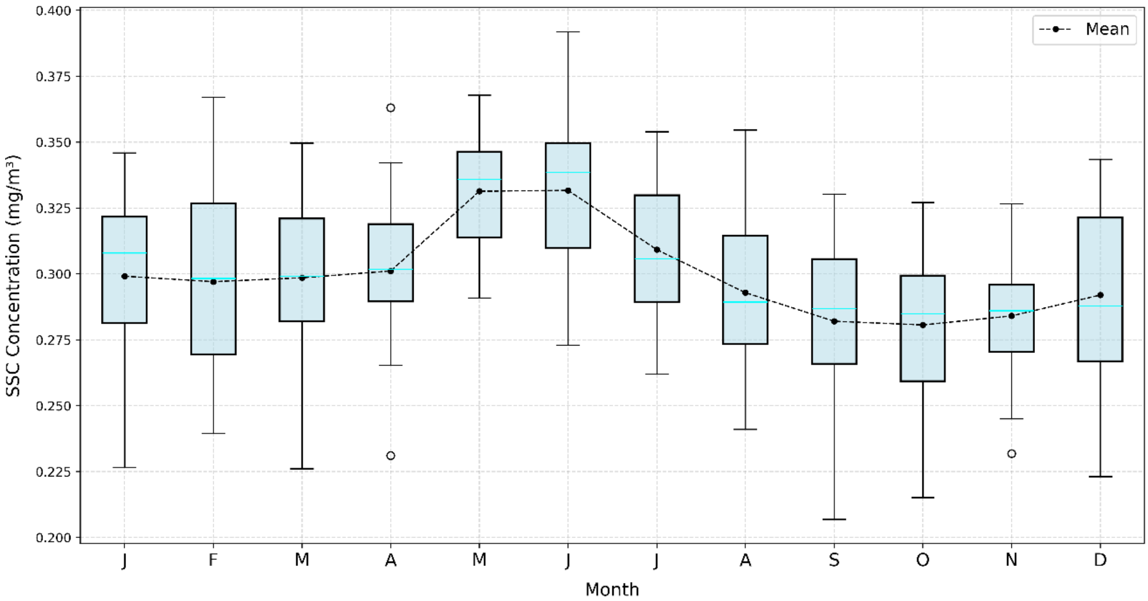

Fig. 3 Box plot of monthly-and-spatially-averaged SSC throughout the study period

The dynamics associated with the asymmetry of SSC dynamics might be primarily driven by the interannual modulation of large-scale climate forcing, particularly ENSO (Subardjo et al., 2017; Leung et al., 2019), which alters the magnitude, timing, and spatial distribution of SSC blooms, primarily by influencing wind patterns, upwelling, SST, and river discharge. The high variability observed during the primary bloom season (May-July) likely reflects the ecosystem's acute sensitivity to the strength of ENSO events during this period. For example, strong El Niño conditions can enhance upwelling or mixing in the eastern Indonesian seas (Subardjo et al., 2017), leading to anomalously high nutrient supply and a strong phytoplankton bloom, while strong La Niña events can cause intense stratification and suppress productivity, leading to a weak bloom. This year-to-year fluctuations of varying conditions induced by ENSO would therefore manifest as the large IQR observed during particular months.

Conversely, the exceptional consistency of the annual SSC minimum in October suggests a seasonal relaxation of these strong interannual drivers. During this period, the system may consistently return to a baseline state governed by strong thermal stratification and pervasive nutrient limitation, where deep chlorophyll-a maxima (DCM) at the subsurface commonly observed (Viljoen et al., 2022; Liang et al., 2020). This certainly results in a predictable low-biomass condition with minimal year-to-year variation because the primary limiting factors are stable, regardless of the preceding ENSO state. The secondary winter bloom's moderate variability could be influenced by other, also variable, drivers such as the intensity of monsoonal winds or the volume of riverine discharge (Menon et al., 2019; Devlin et al., 2018). In essence, the box plot reveals the ecosystem's differential sensitivity to environmental forcing, highlighting a predictable baseline state and a highly variable, ENSO-modulated productive season.

4. Monthly SST Climatology

The monthly climatological maps of SST reveal a distinct and spatially warm and quasi-homogenous seasonal cycle in NPS, which is due to the nature of the location within the WPWP (Bassinot et al., 2000). The region experiences its warmest surface conditions in two distinct periods. A primary warming peak occurs during the boreal fall, where climatological averaged SSTs shows value of 29.59°C, particularly in a band trapped along the Papuan coast. A secondary warm period is observed during boreal winter, where throughout NPS, sea surface warms to 29.53°C. Conversely, the most prominent cooling occurs during the boreal summer. During the season, the climatological SST dropped to 29.07°C. A significant mass of cooler water, with temperatures dropping below 28°C (as shown on Fig. 4), is observed intruding into the study area from the southwest. This intrusion creates a strong cross-shelf temperature gradient that is not apparent during the rest of the year. The overall seasonal range across the domain is approximately 2-3°C, a significant thermal variation for this equatorial region.

The mechanisms driving this seasonal SST evolution appear to be a complex interplay between local thermodynamics and regional ocean dynamics, largely governed by the monsoons. The pronounced cooling observed during boreal winter, which coincides with the Southeast Monsoon, is unlikely to be caused by local surface heat loss alone. The clear spatial pattern of cooler water entering from the southwest strongly suggests that advection by ocean currents is a primary driver. During boreal summer, NGCC typically flows northwestward along the coast, transporting cooler, higher-latitude waters into the region (Kuroda et al., 2003). This advective cooling which possibly coincides with the local upwelling along the coast provides a theoretical explanation for the observed SST drop. In contrast, the peak warming during the October-December inter-monsoon period likely results from the weakening of NGCC, which is associated with gradual changes of the prevailing wind shift (Wu et al., 2020), thus resulting in reduced NGCC's velocity. This allows the surface layer to absorb and retain significant heat. This dynamic, where seasonal patterns are shaped by both large-scale advection and local thermodynamic forcing, underscores the complexity of the physical environment that modulates the region's marine ecosystem.

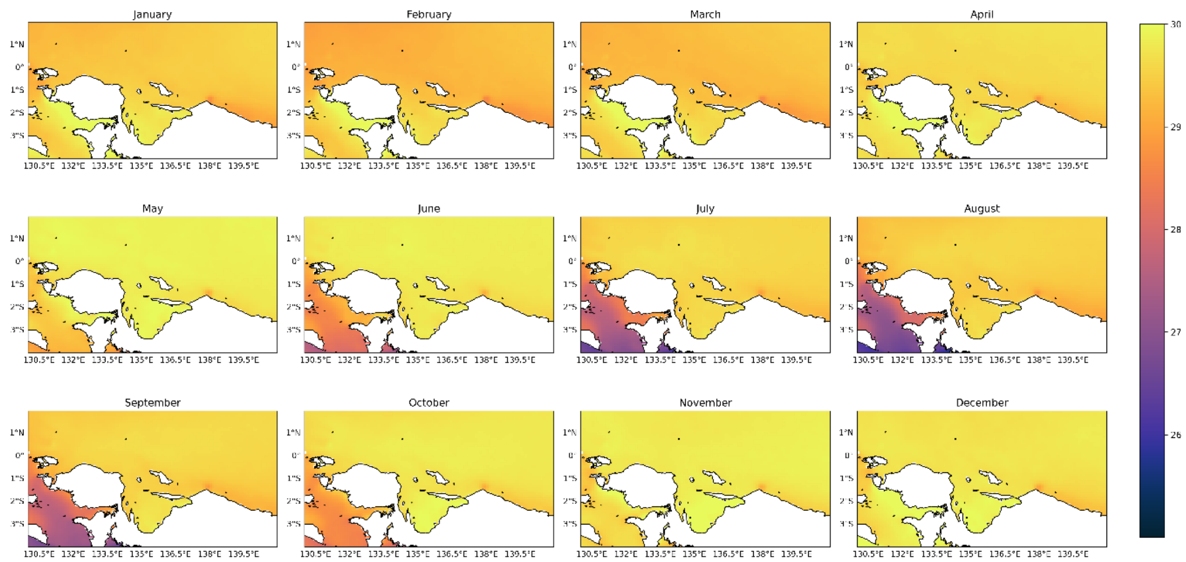

Fig. 4 Spatial distribution of monthly climatological SST

A comparative analysis of the monthly SSC and SST climatology reveals a spatially coherent inverse relationship, which varies in intensity throughout the year. During the boreal summer, the intrusion of cooler SSTs (<28°C) from the southwest into the study domain spatially corresponds with the period of the most widespread and intense SSC concentrations. Moreover, the state of the region being influenced by the cooler waters is where the seasonal chlorophyll bloom appears most pronounced. Conversely, during the late-year warming peak (October-December), when coastal SSTs consistently exceed 30°C, the spatial extent of high SSC contracts significantly, and most of the domain returns to oligotrophic conditions. This opposing spatial and temporal phasing between the two parameters provides strong visual evidence for an inverse coupling, where cooler surface conditions are geographically associated with higher phytoplankton biomass and vice-versa.

The mechanisms driving this distinct inverse spatial patterning are likely rooted in the dominant control of SST over upper ocean stratification and nutrient availability (Watanabe et al., 2020). The widespread of the warm surface waters characteristic in WPWP for most of the year maintain a strong thermal stratification that acts as a barrier to vertical nutrient mixing, resulting in the vast oligotrophic areas with low SSC seen in the maps. The seasonal cooling event during the boreal summer, likely driven by the advection of cooler water via NGCC and enhanced monsoonal winds, weakens this stratification. This process allows for the upward flux of nutrients, which further strengthening the widespread phytoplankton blooms mostly observed in those cooler regions. However, an interesting nuance is observed in the immediate coastal zones. Here, persistently high SSC can coincide with the warmest coastal SSTs, particularly near river mouths. This suggests that in these nearshore areas, terrestrial nutrient input from riverine discharge can be sufficient to override the limiting effects of thermal stratification, creating a system where phytoplankton growth is less dependent on temperature-mediated vertical mixing and more on the direct supply of land-based nutrients.

5. Observed Long-Term Trends of SSC and its driver

A visual comparison of the monthly SSC anomaly time series (Fig. 5a) with ONI (Fig. 6b) reveals a moderate positive relationship over the period. Prolonged periods of negative SSC anomalies, which indicates higher phytoplankton biomass, are clearly aligned with significant La Niña events (negative ONI). For example, the extended La Niña from mid-1998 to early 2001 corresponds to a sustained period of negative SSC anomalies. Conversely, some of the periods of significant positive SSC anomalies coincide with major El Niño events (positive ONI). This is most evident during the El Niño onset in 2015-2016, which corresponds to positive anomalies in the entire SSC record. The lagged cross-correlation analysis (Fig. 5c) quantifies the relationship, revealing that the correlation strength is highest at a lag of approximately 2 months, with the ONI leading the SSC response. The peak correlation coefficient reaches a value of 0.31. This lag suggests a delayed response of the local SSC with the large-scale forcing induced by ENSO, revealing insight into the teleconnection between the two proxies.

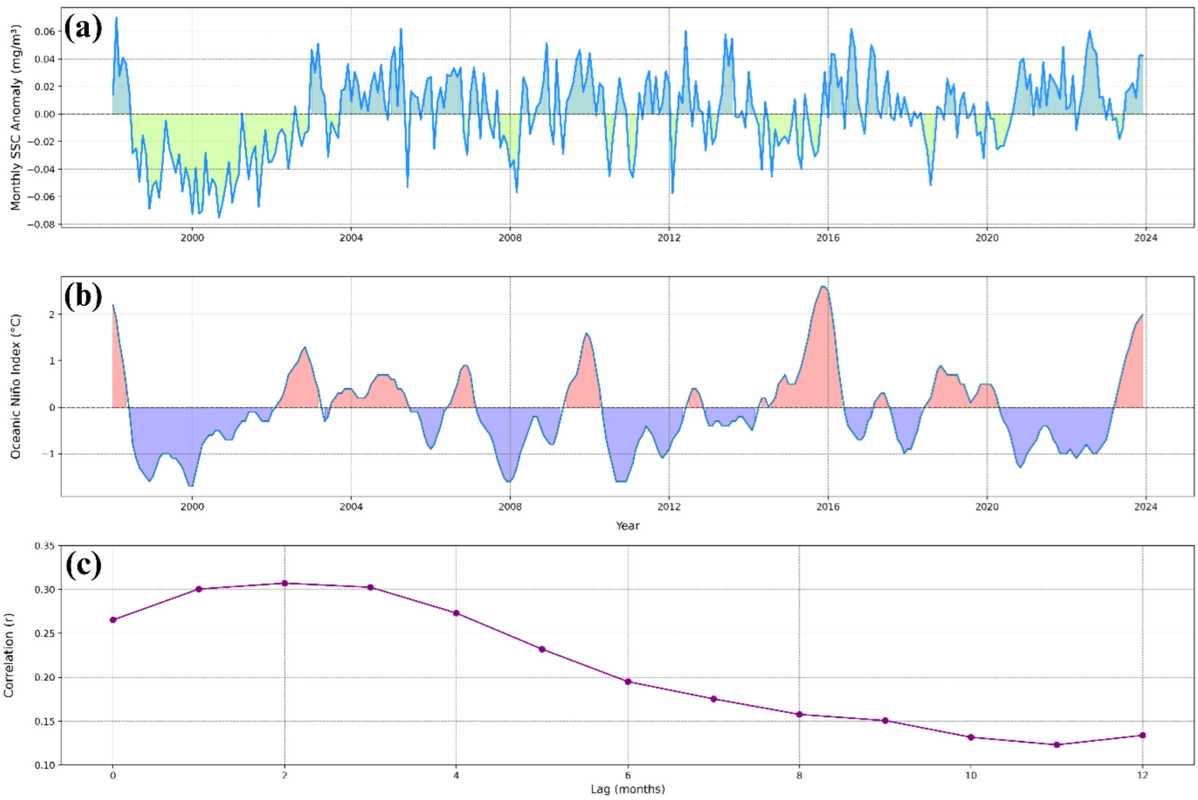

Fig. 5 Time series of (a) climatological monthly SSC anomaly, (b) Oceanic Nino Index (ONI), and (c) lag correlation ranging from 0-12 months

The robust inverse correlation and 2-month lag between ONI and regional SSC strongly indicates that ENSO is a primary modulator of interannual phytoplankton dynamics in the Northern Papua Sea. The underlying mechanism is likely driven by ENSO's influence on regional ocean physics. During La Niña phases, WPWP often experiences anomalous warming and a deepening of the thermocline (Cao et al. 2023). This leads to enhanced thermal stratification of the upper water column, which acts as a barrier, isolating the vertical flux of essential nutrients from the subsurface to the euphotic zone and thereby suppressing phytoplankton growth (Hoteit et al. 2018) and leading to negative SSC anomalies. During El Niño phases, the opposite occurs: a shoaling of the thermocline and cooler surface waters weaken stratification, which enhances nutrient supply through mixing or upwelling and fuels periods of higher-than-average phytoplankton biomass. The observed 2-month lag is physically meaningful, representing the characteristic timescale required for the large-scale atmospheric and oceanic anomalies associated with ENSO to propagate from the central Pacific and manifest as significant changes in the local oceanographic conditions of NPS.

The overall correlation coefficient between the monthly SST and SSC anomaly time series for the entire study period is r = -0.22 (annotated in Fig. 6), indicating a weak and negative linear association when considering all scales of variability. However, the opposing nature of the linear trends themselves provides stronger evidence for a long-term inverse coupling, suggesting that as regional SST have risen, surface phytoplankton biomass has tended to decline. This pattern implies that the mechanisms driving the warming trend also promote conditions less favorable for SSC accumulation in NPS.

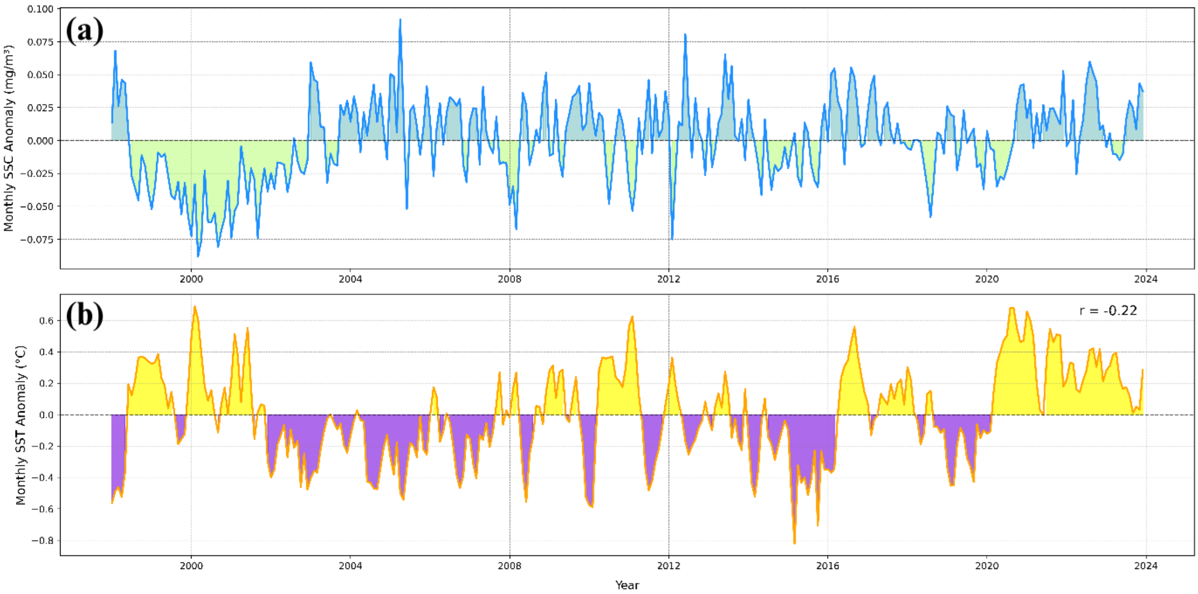

Fig. 6 The time series of climatological monthly (a) SSC and (b) SST anomaly with annotated correlations

While the inverse correlation between SST and SSC is the main characteristic of NPS' ecosystem, its consistency across multiple timescales suggests that the system is fundamentally nutrient-limited. In this regime, the indirect physical effects of SST on the water column structure—primarily its control over stratification—dominate over any direct physiological enhancement of phytoplankton growth from warmer temperatures. Therefore, in this context, SST should be interpreted not only as a direct thermal stressor but also as a powerful proxy for the physical conditions governing nutrient availability to the surface layer. Deviations from this relationship, although not dominant in our long-term analysis, could indicate periods where other processes, such as major river discharge events or anomalous wind-driven mixing, temporarily disrupt this primary controlling mechanism.

The observed coastal-offshore dichotomy in long-term SSC trends suggests that different environmental drivers are dominant in these two distinct regimes, leading to opposing ecosystem responses over the past two decades. The significant increase in SSC along the coast, occurring despite regional sea surface warming, points towards a powerful local or regional nutrient enrichment mechanism that is overriding the negative effects of thermal stratification. This is potentially driven by changes in terrestrial and riverine discharge from the large landmass of Papua. Long-term changes in regional rainfall patterns, land-use practices such as deforestation or agriculture, and coastal development could be increasing the flux of nutrients and organic matter into the coastal zone (Kovar et al. 2020; Webb et al. 2019), thereby enhancing phytoplankton productivity.

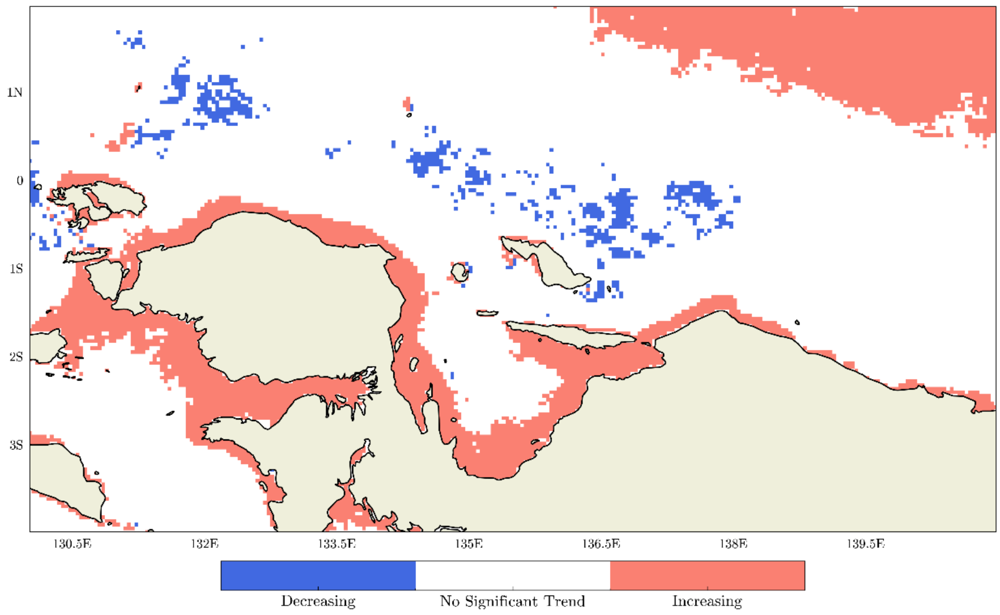

Fig. 7 The result of modified Mann-Kendall test

Conversely, the significant decreasing trend in SSC observed in patches of the open ocean aligns with the expected theoretical response of oligotrophic systems to global climate change (Tian & Zhang 2023). In these offshore areas, far from direct terrestrial influence, the persistent warming of the sea surface enhances upper-ocean stratification. This strengthening of the physical barrier between the sunlit surface and deeper, nutrient-rich waters leads to a long-term reduction in vertical nutrient supply, a process often termed "oligotrophication," which results in declining phytoplankton biomass. Therefore, NPS appears to be a region experiencing two concurrent but opposing long-term pressures: a potential "greening" of the coastal zone likely driven by terrestrial inputs, and a "bluing" of the offshore waters driven by climate-induced stratification.

In addition, the resulting CV spatial map (Fig. 8) reveals a striking heterogeneity in SSC variability, clearly delineating between highly dynamic coastal zones and more quiescent offshore waters. The most pronounced relative variability, with CV values frequently exceeding 80%, is concentrated in southeastern coastal of NPS. A particularly large zone of high variability is evident along the NPS' coast, between approximately 137°E and 139.5°E, with other significant patches located within the complex archipelagic waters near 132°E and 135°E. In sharp contrast, the open-ocean regions, especially north of the equator, exhibit significantly lower relative variability (CV $< 40\%$). This pattern creates a distinct gradient, with variability generally decreasing with distance from the coast, effectively partitioning the study area into a highly variable coastal regime and a more stable offshore system.

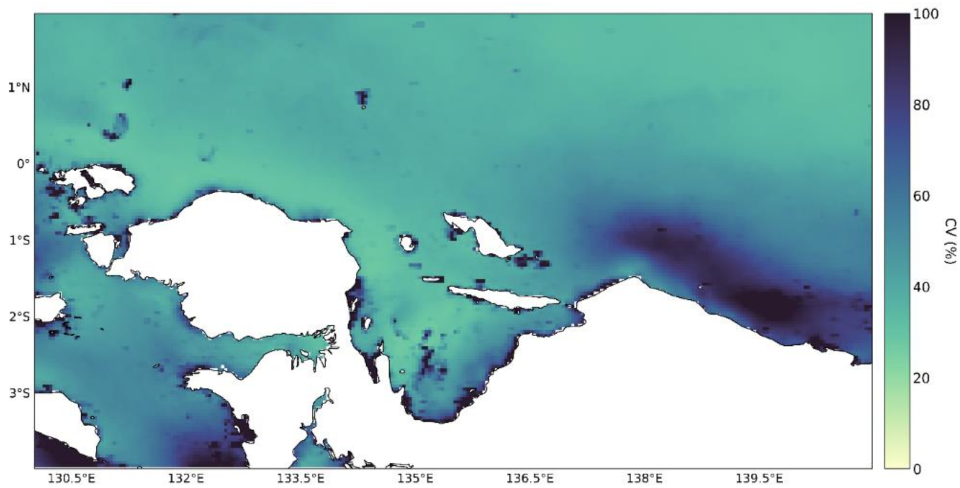

Fig. 8 Coefficient of variation (CV) of SSC

The spatial dichotomy in SSC variability highlighted by the CV analysis indicates that the dominant environmental drivers differ significantly between the coastal and offshore regimes. The high CV observed along the coast is likely a signature of strong, episodic forcing that induces large, intermittent phytoplankton blooms over a baseline concentration. The heightened variability near the coast is potentially caused by modulating factors beyond the scope of study, namely tidal range which affect the resuspension of nutrients (Kitsiou & Kotta 2019). Additionally, the influence of precipitation can drive localized nutrient input, particularly in estuaries and coastal zones (Liu et al., 2023), further contributing to the high year-to-year variability in bloom intensity and timing. Conversely, the low CV in the offshore waters is characteristic of the stable, strongly stratified, and oligotrophic conditions of the WPWP (Panighari et al., 2020). Far from direct terrestrial influence, this offshore regime is governed by slower, large-scale ocean dynamics, where consistently low nutrient availability suppresses the potential for large blooms, resulting in low absolute and relative variability.

6. Multi-Scale Variability and Periodicity

The CWT analysis provides a deep insight into the multi-scale temporal dynamics of NPS, revealing a complex and non-linear relationship between the large-scale climate forcing represented by ONI, the regional physical response in SST, and SSC (Fig. 9). The wavelet spectrum of the ONI (Fig. 8c) serves as a clear benchmark, exhibiting its well-known, statistically significant power concentrated in the 16 to 64 month interannual band, with high-energy spectrum corresponding directly to major climate events such as the strong interannual periodicity exhibited during the period of 2003-2020, which include the series of El Niño events from 2010-2012, and the major El Niño of 2014-2016. However, this forcing signal doesn't reflect the dynamics in the regional SST spectrum (Fig. 8b), which displays a persistent and significant band of power across semi-annual (~4-8 months) period for nearly the entire record. This strong incorrespondence confirms that the physical thermal environment of NPS is significantly modulated by phenomenon other than ENSO forcing that may confluence the local SST variability. Karang et al. (2019) suggested that the SST in NPS also responds to regular seasonal and 6-monthly cycles, with distinct warming and cooling phases linked to broader regional climate patterns and solar radiation changes.

In contrast, the biological system's response is markedly more selective and episodic. The SSC wavelet spectrum (Fig. 8a) shows significant power in this interannual band only during discrete, high-amplitude events; for instance, while SST shows continuous significant variability throughout the period, SSC only exhibits a significant response intermittently. The most notable SSC responses are concentrated during the most intense climate phases, such as the prolonged La Niña at the start of the record and the major El Niño of 2015-2016. Furthermore, the SSC spectrum reveals significant power at the annual to quasi-annual scale (~12-16 months) especially between 1999 and 2002, a feature which less prominent in the ONI spectrum. This complex behavior suggests that while

ENSO sets the primary tempo for interannual variability, the regional phytoplankton community responds in a non-linear fashion, perhaps only when the physical forcing crosses a critical intensity threshold, or when the large-scale ENSO forcing constructively interferes with local, higher-frequency drivers such as monsoonal wind patterns or river discharge cycles.

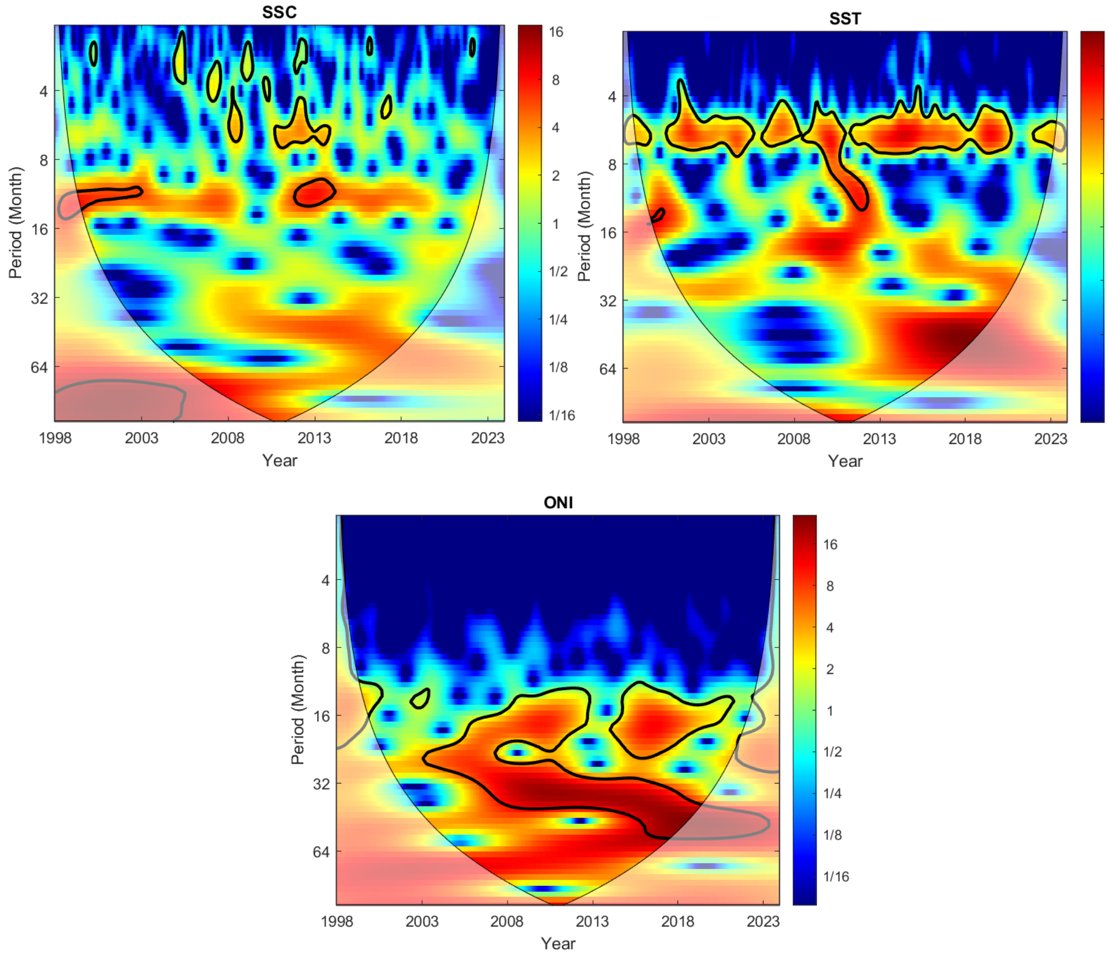

Fig. 9 The result of continuous wavelet transforms (CWT) of SSC, SST, and ONI

The XWT analysis further extend the investigation of the periodicity between the proxies and was employed to quantitatively examine the coupled variability and time-frequency specific phase relationships between the monthly SST, SSC, and ONI from 1998 to 2023 (Fig. 10). The analysis between the ONI and regional SST (Fig. 10c) reveals a robust and persistent region of significant power centered in the 1–4 year interannual band. This high coherence is particularly strong during the major ENSO cycles of 2008-2013 and 2014-2018, which each of them coincides with 1-2 year and 1–4 year periodicity, respectively. Within these significant regions, the phase arrows point consistently to the right, indicating a clear anti-phase relationship, where positive ONI values directly correspond to negative regional SST anomalies. The XWT between SST and SSC (Fig. 9a) also identifies significant common power, concentrated primarily in the semi-annual band but manifesting more episodically. Strong consistent coherence is evident during the period, around 2010-2020, and the remaining shows episodic coherence, notably during the 1999 and 2013 where the plot shows stronger coherence. Crucially, the phase arrows in these regions point exhibit variable coherence, demonstrating variability across multiple timescales. A slight but consistent clockwise tilt in these arrows notably during events like the 2010-2012 period further suggests that SST variations tend to lead the anti-phase SSC response. Lastly, this inverse coupling is corroborated by the XWT between the large-scale ENSO forcing and regional SSC (Fig. 9b). Here, significant coherence is again exhibiting episodic coherence, where the periodicity varies from semi-annual into interannual scale. concentrated in the ~8-16 month and ~32-64 month band, with the phase arrows also progressively clockwise tilting from left, highlighting that ENSO phases are not always in phase with SSC dynamics.

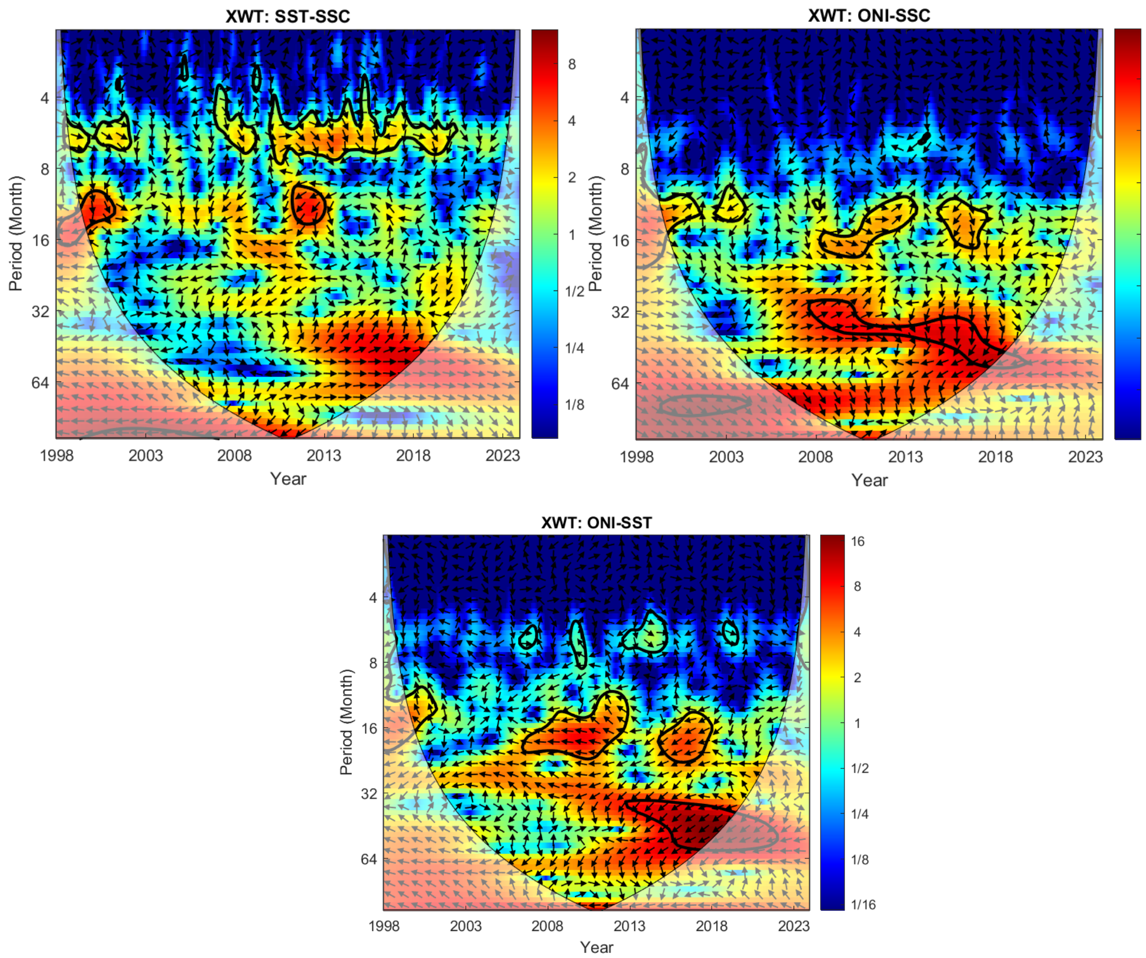

Fig. 10 The results of cross wavelet transform (XWT) of SST-SSC, ONI-SSC, ONI-SST

The wavelet analysis presents a nuanced picture of the environmental dynamics in NPS, where the regional SST and SSC exhibit different responses to large-scale climate forcing. A surprising key finding is the apparent decoupling of the dominant periodicities between regional SST and the large-scale ENSO forcing. While the ONI is characterized by its well-known 2-7 year interannual variability, the regional SST spectrum is instead dominated by a persistent and significant semi-annual (~4-8 month) cycle throughout the study period. This strong semi-annual signal, which is absent in the ONI, suggests that the primary rhythm of thermal variability in this specific region is governed by regional-scale processes rather than being a direct reflection of ENSO. This cycle may be linked to the bi-annual monsoonal regime (Wijaya et al. 2024; Karang et al. 2019), which drives semi-annual shifts in wind stress, cloud cover and solar insolation, and potentially the advection of distinct water masses via the NGCC. Although ENSO's interannual influence is present, its power in the SST spectrum is secondary to this more dominant regional semi-annual cycle.

In contrast, the SSC response is markedly more episodic and appears slightly more attuned to the interannual ENSO signal than the semi-annual SST cycle. The SSC wavelet spectrum shows significant power in the interannual band only during discrete, high-amplitude climate events, such as the major El Niño of 2014-2016. This suggests that the phytoplankton community is resilient to moderate physical fluctuations but exhibits a strong, non-linear response when a climatic forcing, like a major ENSO event, crosses a critical intensity threshold (Zhuang et al. 2020; Li et al. 2020; Tagliabue et al. 2010). This threshold-based dynamic could explain why not every warm or cool period in the SST record triggers a significant biological response. Furthermore, the presence of significant annual to interannual power in the SSC spectrum, particularly in the early 2000s, which does not have a strong counterpart in the ONI, indicates that local interannual processes, such as peak river discharge cycles (Deser et al. 1989) or specific phases of the monsoon (Wang et al. 2021), also play a crucial role in modulating phytoplankton blooms, independent of the larger ENSO state.

The XWT analysis further clarifies these complex interactions by revealing the phase relationships between the drivers and responses. Crucially, the XWT confirms a strong in-phase coherence between ONI and regional SST at interannual periods, indicating that La Niña onset correspond to anomalously warm conditions in the study area. This establishes a direct link for the physical teleconnection, even if it is not the dominant mode of local SST variability. However, the relationship between SST and SSC is more complex. The XWT between SST and SSC shows that their strongest and most consistent coherence occurs in the semi-annual band, reinforcing the idea that the ecosystem is highly responsive to this regional-scale physical cycle. Within these coherent periods, the phase arrows often exhibit a clockwise tilt from an anti-phase position, suggesting that SST variations tend to lead the inverse SSC response, which aligns with a process where physical changes in the environment precede a biological reaction.

The connection between the large-scale ENSO forcing and the SSC is episodic and multi-faceted. Significant coherence appears at various periodicities, from the semi-annual to the interannual scale, and the phase relationship is not fixed. The arrows often show a progressive clockwise tilt away from a pure anti-phase (left-pointing) relationship, highlighting that the biological response to ENSO is complex and not always perfectly inverse. This reinforces the hypothesis that the local ecosystem response is a composite of multiple influences. The basin-wide ENSO signal provides a powerful, low-frequency 'push' during major events, but the resulting biological outcome is heavily modulated by the phase and strength of the regional semi-annual thermal cycle and other local drivers, leading to the complex and variable phase relationships observed in the XWT analysis.

Conclusion

The analysis of 26 years of satellite-derived data for NPS has revealed a statistically significant, coupled long-term shift in the region's baseline biophysical state. Persistent warming trend in SST is documented, and concurrent with a significant decline in SSC. One of the dominant mode of interannual variability for SSC and SST was unambiguously linked to the ENSO, with a robust in-phase and anti-phase relationship characterizing their coupled response. The following discussion aims to elucidate the potential mechanisms driving these observed dynamics and consider their broader ecological implications.

The consistent inverse coupling between SST and SSC across multiple timescales, from seasonal cycles to major interannual events, strongly suggests that the surface phytoplankton biomass in this oligotrophic region is fundamentally controlled by nutrient availability, which is in turn modulated by physical processes. The wavelet coherence analysis demonstrated that warmer SST anomalies, particularly during strong El Niño events, are robustly associated with suppressed SSC. This provides compelling evidence that enhanced thermal stratification during warm periods is the principal mechanism at play, inhibiting vertical mixing and limiting the nutrient supply to the euphotic zone, thereby overriding any direct physiological enhancement of phytoplankton growth from warmer temperatures.

This study addresses a significant knowledge gap by providing a comprehensive, multi-decadal characterization of coupled SSC-SST dynamics in the under-characterized NPS. However, the reliance on satellite observations means the findings are inherently surface-biased and do not capture subsurface ocean dynamics. Future investigations should, therefore, prioritize the integration of in-situ observations and coupled physical-biogeochemical models to explore the three-dimensional structure of chlorophyll-a, particularly the role of deep chlorophyll maxima (DCMs). Elucidating the full water column response is a critical next step to fully comprehend the resilience and future trajectory of this vital marine ecosystem in the face of continued climate change.

Acknowledgements The author gratefully acknowledges the editor and anonymous reviewers for their constructive suggestions and encouraging feedback, which significantly improved the quality of this manuscript. The author acknowledges the use of Google Gemini (Version 2.5) to assist with paragraph structure and coherent flow refinement throughout this manuscript, but did not contribute to the core ideas or scientific analysis

presented. The author assumes full responsibility for the final text. All figures presented in this study were generated using Python, MATLAB, and Surfer.

Funding The author received no financial support, grants, or funding during the preparation of this manuscript.

Declarations

Ethics approval and consent to participate Not applicable.

Consent for publication Not applicable.

Competing interests The authors declare no competing interests.

Human ethics Not applicable

Data Availability Statement The datasets analysed during the current study are publicly available from the following sources. Sea Surface Chlorophyll-a (SSC) concentration data were obtained from the Copernicus Marine Service (CMS) and are available at https://doi.org/10.48670/moi-00281. Sea Surface Temperature (SST) data were also sourced from the Copernicus Marine Service (CMS), available at https://doi.org/10.48670/mds-00345. The Oceanic Niño Index (ONI) data were retrieved from NOAA's Climate Prediction Center, available at https://origin.cpc.ncep.noaa.gov/products/analysis_monitoring/ensostuff/ONI_v5.php.

References

Balch, C. (2021). Exploring Sea Surface Temperature's Effect on Global Ocean Productivity in Our Changing Climate. *Inquiry Journal, University of New Hampshire*.

Bassinot, F., Garidel-Thoron, T., Rosenthal, Y., & Beaufort, L. (2005). Stable sea surface temperatures in the western Pacific warm pool over the past 1.75 million years. *Nature*, 433, 294-298. https://doi.org/10.1038/nature03189.

Bonnet, S., Guieu, C., Bruyant, F., Prášil, O., Wambeke, F., Raimbault, P., Moutin, T., Grob, C., Gorbunov, M., Zehr, J., Masquelier, S., Garczarek, L., & Claustre, H. (2007). Nutrient limitation of primary productivity in the Southeast Pacific (BIOSOPE cruise). *Biogeosciences*, 5, 215-225. https://doi.org/10.5194/BG-5-215-2008.

Cao, Z., Wang, D., Gordon, A., Li, M., & Zheng, F. (2023). Roles of the Indo-Pacific subsurface Kelvin waves and volume transport in prolonging the triple-dip 2020–2023 La Niña. *Environmental Research Letters*, 18. https://doi.org/10.1088/1748-9326/acfcce.

Chen, D., Lian, T., Fu, C., Cane, M., Tang, Y., Murtugudde, R., Song, X., Wu, Q., & Zhou, L. (2015). Strong influence of westerly wind bursts on El Niño diversity. *Nature Geoscience*, 8, 339-345. https://doi.org/10.1038/NGEO2399.

Chernihovsky, N., Almogi-Labin, A., Kienast, S., & Torfstein, A. (2020). The daily resolved temperature dependence and structure of planktonic foraminifera blooms. *Scientific Reports*, 10. https://doi.org/10.1038/s41598-020-74342-z.

Cloern, J. E., Foster, S. Q., & Kleckner, A. E. (2014). Phytoplankton primary production in the world's estuarine-coastal ecosystems. *Biogeosciences, 11*(9), 2477–2501.

De Poll, V., Kulk, G., Timmermans, K., Brussaard, C., Woerd, H., Kehoe, M., Mojica, K., Visser, R., Rozema, P., & Buma, A. (2013). Phytoplankton chlorophyll a biomass, composition, and productivity along a temperature and stratification gradient in the northeast Atlantic Ocean. *Biogeosciences*, 10, 4227-4240. https://doi.org/10.5194/BG-10-4227-2013.

Deser, C., Richey, J., & Nobre, C. (1989). Amazon River Discharge and Climate Variability: 1903 to 1985. *Science*, 246, 101 - 103. https://doi.org/10.1126/science.246.4926.101.

Deser, C., Alexander, M., & Timlin, M. (2003). Understanding the persistence of sea surface temperature anomalies in midlatitudes. *Journal of Climate*, 16, 57-72. https://doi.org/10.1175/1520-0442(2003)016<0057:UTPOSS>2.0.CO;2.

Devlin, A., Yan, Y., Shen, C., Pan, J., & Zhao, H. (2018). Influence of monsoonal winds on chlorophyll-α distribution in the Beibu Gulf. *PLoS ONE*, 13. https://doi.org/10.1371/journal.pone.0191051.

Dwirastina, M., & Atminarso, D. (2021). Evaluation of the Conditions of Mamberamo River Water with Biomass and Phytoplankton Community Approach. *Jurnal Ilmiah Perikanan Dan Kelautan*, 13(1), 38–47. https://doi.org/10.20473/jipk.v13i1.17565

Falkowski, P. (1994). The role of phytoplankton photosynthesis in global biogeochemical cycles. *Photosynthesis Research*, 39, 235-258. https://doi.org/10.1007/BF00014586.

Fedorov, A., Hu, S., Lengaigne, M., & Guilyardi, E. (2015). The impact of westerly wind bursts and ocean initial state on the development, and diversity of El Niño events. *Climate Dynamics*, 44, 1381-1401. https://doi.org/10.1007/s00382-014-2126-4.

Garnesson, P., Mangin, A., Fanton d'Andon, O., Demaria, J., & Bretagnon, M. (2019). The CMEMS GlobColour chlorophyll a product based on satellite observation: multi-sensor merging and flagging strategies. Ocean Science, 15(3), 819–830. https://doi.org/10.5194/os-15-819-2019

Gittings, J., Raitsos, D., Krokos, G., & Hoteit, I. (2018). Impacts of warming on phytoplankton abundance and phenology in a typical tropical marine ecosystem. *Scientific Reports*, 8. https://doi.org/10.1038/s41598-018-20560-5.

Groom, S., Sathyendranath, S., Ban, Y., Bernard, S., Brewin, R., Brotas, V., Brockmann, C., Chauhan, P., Choi, J., Chuprin, A., Ciavatta, S., Cipollini, P., Donlon, C., Franz, B., He, X., Hirata, T., Jackson, T., Kampel, M., Krasemann, H., … Wang, M. (2019). Satellite Ocean Colour: Current Status and Future Perspective. Frontiers in Marine Science, 6. https://doi.org/10.3389/fmars.2019.00485

Hasegawa, T., Ando, K., Mizuno, K., & Lukas, R. (2009). Coastal upwelling along the north coast of Papua New Guinea and SST cooling over the pacific warm pool: A case study for the 2002/03 El Niño event. *Journal of Oceanography*, 65, 817-833. https://doi.org/10.1007/S10872-009-0068-Y.

Henebry, G., & De Beurs, K. (2005). Land surface phenology and temperature variation in the International Geosphere–Biosphere Program high-latitude transects. *Global Change Biology*, 11. https://doi.org/10.1111/j.1365-2486.2005.00949.x.

Hoteit, I., Gittings, J., Krokos, G., & Raitsos, D. (2018). Impacts of warming on phytoplankton abundance and phenology in a typical tropical marine ecosystem. *Scientific Reports*, 8. https://doi.org/10.1038/s41598-018-20560-5.

Hu, S., & Fedorov, A. (2019). The extreme El Niño of 2015–2016: the role of westerly and easterly wind bursts, and preconditioning by the failed 2014 event. *Climate Dynamics*, 52, 7339-7357. https://doi.org/10.1007/s00382-017-3531-2.

Hussain, Md., & Mahmud, I. (2019). pyMannKendall: a python package for non parametric Mann Kendall family of trend tests. *Journal of Open Source Software*, 4(39), 1556. https://doi.org/10.21105/joss.01556

Karang, I., Putra, I., & Putra, I. (2019). Analisis Temporal Suhu Permukaan Laut di Perairan Indonesia Selama 32 Tahun (Era AVHRR). *Journal of Marine and Aquatic Sciences*. https://doi.org/10.24843/jmas.2019.v05.i02.p11.

Khalil, I., Mannaerts, C.M., Ambarwulan, W. (2009). Distribution of chlorophyll-a and sea surface temperature (SST) using MODIS data in East Kalimantan waters, Indonesia. *Journal of Sustainability Science and Management, 4*(2), 125-140.

Kitsiou, D., & Kotta, D. (2019). Chlorophyll in the Eastern Mediterranean Sea: Correlations with Environmental Factors and Trends. *Environments*. https://doi.org/10.3390/ENVIRONMENTS6080098.

Kovar, K., Kronvang, B., Fraters, D., & Wendland, F. (2020). Land Use and Water Quality. *Water*. https://doi.org/10.3390/w12092412.

Kuroda, Y., Kashino, Y., & Ueki, I. (2003). Observation of current variations off the New Guinea coast including the 1997-1998 El Nino period and their relationship with Sverdrup transport. *Journal of Geophysical Research*, 108, 3243. https://doi.org/10.1029/2002JC001611.

Leung, S., Iskandar, I., Wirasatriya, A., Setiawan, R., & Hernawan, U. (2019). Spatio-temporal variability of surface chlorophyll-a in the Halmahera Sea and its relation to ENSO and the Indian Ocean Dipole. *International Journal of Remote Sensing*, 41, 284 - 299. https://doi.org/10.1080/01431161.2019.1641244.

Li, T., Pan, D., Zhang, Z., Chen, X., Dang, X., He, X., Chen, C., & Bai, Y. (2020). Impact of ENSO events on phytoplankton over the Sulu Ridge. *Marine environmental research*, 157, 104934 . https://doi.org/10.1016/j.marenvres.2020.104934.

Liang, J., Tian, Z., Sun, X., Zhao, Y., Li, X., Zhu, M., Dai, S., Liu, H., & Wang, Z. (2020). The seamount effect on phytoplankton in the tropical western Pacific.. *Marine environmental research*, 162, 105094 . https://doi.org/10.1016/j.marenvres.2020.105094.

Litchman, E., Pinto, T., Edwards, K., Klausmeier, C., Kremer, C., & Thomas, M. (2015). Global biogeochemical impacts of phytoplankton: a trait-based perspective. *Journal of Ecology*, 103. https://doi.org/10.1111/1365-2745.12438.

Liu, Z., He, S., Li, P., Gu, Y., Zhai, F., & Hao, Q. (2023). Satellite-observed interannual variations in sea surface chlorophyll-a concentration in the Yellow Sea over the past two decades. *Journal of Geophysical Research: Oceans*. https://doi.org/10.1029/2022jc019528.

Marañón, E., et al. (2022). Phytoplankton responses to changing temperature and nutrient availability are consistent across the tropical and subtropical Atlantic. *Communications Biology, 5*(1), 1019.

Menon, N., Balchand, A., Platt, T., Shafeeque, M., Shah, P., George, G., & Sathyendranath, S. (2019). Effect of Precipitation on Chlorophyll-a in an Upwelling Dominated Region Along the West Coast of India. *Journal of Coastal Research*, 86, 218 - 224. https://doi.org/10.2112/SI86-032.1.

Naselli-Flores, L., & Padisák, J. (2022). Ecosystem services provided by marine and freshwater phytoplankton. *Hydrobiologia*, 850, 2691 - 2706. https://doi.org/10.1007/s10750-022-04795-y.

Panigrahi, M., Gupta, A., Mohan, K., Bali, H., Thirumalai, K., & Tiwari, S. (2020). Evolution of the Oligotrophic West Pacific Warm Pool During the Pliocene-Pleistocene Boundary. *Paleoceanography and Paleoclimatology*, 35. https://doi.org/10.1029/2020PA003875.

Pilon, P., & Yue, S. (2004). A comparison of the power of the t test, Mann-Kendall and bootstrap tests for trend detection / Une comparaison de la puissance des tests t de Student, de Mann-Kendall et du bootstrap pour la détection de tendance. *Hydrological Sciences Journal*, 49, 21 - 37. https://doi.org/10.1623/hysj.49.1.21.53996.

Napitupulu, G. (2024). Monthly variability of wind-induced upwelling and its impact on chlorophyll-a distribution in the Southern and Northern parts of the Indonesian Archipelago. *Ocean Dynamics*, 74(12), 10.1007/s10236-024-01640-9.

Sachoemar, S. I., Yanagi, T., Aliah, R.S. (2001). Variability of Sea Surface Chlorophyll-a, Temperature and Fish Catch within Indonesian Region Revealed by Satellite Data. *Proceedings of the 22nd Asian Conference on Remote Sensing*, *37*(2), 75-87.

Subardjo, P., Wirasatriya, A., & Setiawan, R. (2017). The Effect of ENSO on the Variability of Chlorophyll-a and Sea Surface Temperature in the Maluku Sea. *IEEE Journal of Selected Topics in Applied Earth Observations and Remote Sensing*, 10, 5513-5518. https://doi.org/10.1109/JSTARS.2017.2745207.

Tagliabue, A., Alvain, S., Masotti, I., Moulin, C., Bopp, L., & Antoine, D. (2010). Large-scale shifts in phytoplankton groups in the Equatorial Pacific during ENSO cycles. *Biogeosciences*, 8, 539-550. https://doi.org/10.5194/BG-8-539-2011.

Tian, F. & Zhang, R. (2023). Decreasing surface chlorophyll in the tropical ocean as an indicator of anthropogenic greenhouse effect during 1998–2020. *Environmental Research Letters*, 18. https://doi.org/10.1088/1748-9326/ace638.

Viljoen, J., Tilstone, G., Brewin, R., Aiken, J., Airs, R., Barlow, R., Lamont, T., Woodward, E., & Harris, C. (2022). Latitudinal variability and adaptation of phytoplankton in the Atlantic Ocean. *Journal of Marine Systems*. https://doi.org/10.1016/j.jmarsys.2022.103844.

Vrede, T., & Tranvik, L. (2006). Iron Constraints on Planktonic Primary Production in Oligotrophic Lakes. *Ecosystems*, 9, 1094-1105. https://doi.org/10.1007/s10021-006-0167-1.

Wang, X., Wang, M., Guan, Z., & Xie, S. (2021). A Common Base Mode of Asian Summer Monsoon Variability across Timescales. *Journal of Climate*, 34, 7359-7371. https://doi.org/10.1175/JCLI-D-20-0856.1.

Watanabe, M., Dunne, J., Toyama, K., Stock, C., Yamamoto, A., Chamberlain, M., Bopp, L., Ziehn, T., Li, H., Santana-Falcón, Y., Aumont, O., Torres, O., Yool, A., Orr, J., Lenton, A., Ilyina, T., Séférian, R., Palmiéri, J., Lovenduski, N., Christian, J., Kwiatkowski, L., Takano, Y., Tagliabue, A., John, J., Tjiputra, J., Schwinger, J., Tsujino, H., & Gehlen, M. (2020). Twenty-first century ocean warming, acidification, deoxygenation, and upper-ocean nutrient and primary production decline from CMIP6 model projections. *Biogeosciences*. https://doi.org/10.5194/bg-17-3439-2020.

Webb, J., Holloway, C., Tait, D., Looman, A., Santos, I., & Maher, D. (2019). Dissolved carbon, greenhouse gases, and δ13C dynamics in four estuaries across a land use gradient. *Aquatic Sciences*, 81, 1-15. https://doi.org/10.1007/s00027-018-0617-9.

Wijaya, Y., Setiyono, H., Wirasatriya, A., Lesmana, P., Haryanti, D., Abdillah, M., Suryoputro, A., & Ismunarti, D. (2024). The Effect of ENSO on Upwelling Intensity in the Seas along the Northern Coast of Papua - Case Study of the 2015–2016 El Niño and the 2010–2011 La Niña Events. *Ecological Engineering & Environmental Technology*. https://doi.org/10.12912/27197050/176505.

Wu, J., Wang, Q., Hu, S., Wang, F., Jia, F., Wang, F., Zhang, L., & Hu, D. (2020). Seasonal and Interannual Variability of the Currents off the New Guinea Coast From Mooring Measurements. *Journal of Geophysical Research: Oceans*. https://doi.org/10.1029/2020jc016242.

Zhuang, J., Zhong, Y., Wang, J., Huang, B., Wang, P., Liu, X., Laws, E., & Zhang, C. (2022). Responses of phytoplankton communities driven by differences of source water intrusions in the El Niño and La Niña events in the Taiwan Strait during the early spring. , 9. https://doi.org/10.3389/fmars.2022.997591.